hoods for our cell culture work: one for *M. mycoides* LC donor cell preparation, one for *M. capricolum*, and one for working with transplant clones.

26. There was no sequence that was unique to *M. capricolum*. Of the 24 reads that did not match the *M. mycoides* LC or *M. capricolum* genome sequences, most were either very short reads (<200 bases) or the result of chimeric clones, which is to be expected owing to the active transposons in *M. mycoides* LC and also as part of library construction. The data for the two transplant clones that were sequenced are posted at the National Center for Biotechnology Information, NIH, NCBI Trace File Archives (accession numbers 1807995910 through 1807998555).
27. M. Tarshis, M. Salman, S. Rottem, *Biophys. J.* **64**, 709 (1993).
28. A. M. Teachman, C. T. French, H. Yu, W. L. Simmons, K. Dybvig, *J. Bacteriol.* **184**, 947 (2002).
29. The murine antibodies were gifts from M. Foecking, T. Martin, K. Wise, and M. Calcutt at the University of Missouri.
30. C. L. Gatlin *et al.*, *Proteomics* **6**, 1530 (2006).
31. We thank C. Merryman, L. Young, and N. Assad-Garcia for many discussions about genome transplantation; and D. Rusch, G. Sutton, S. Yooseph, and J. Johnson for bioinformatics analyses. The bulk of the work was supported by Synthetic Genomics. The proteome analysis was funded in part through the Pathogen Functional Genomics Resource Center, managed and funded by the Division of Microbiology and Infectious Diseases, National Institute of Allergy and Infectious Diseases, NIH, Department of Health and Human Services, and operated by the J. Craig Venter Institute. J.C.V. is Chief Executive Officer and Co-Chief Scientific Officer of Synthetic Genomics, Inc., a privately held entity that develops genomic-driven strategies to address global energy and environmental challenges. H.O.S. is Co-Chief Scientific Officer and on the Board of Directors of Synthetic Genomics, Inc. C.A.H. is Chairman of the Synthetic Genomics, Inc., Scientific Advisory Board. All three of these authors hold Synthetic Genomics, Inc., stock, and the J. Craig Venter Institute owns a significant fraction of Synthetic Genomics, Inc. Following the disclosure policy of this journal, the authors disclose that the Venter Institute has filed for a patent application on some of the techniques described in this paper.

REPORTS

Quantum Hall Effect in a Gate-Controlled *p-n* Junction of Graphene

J. R. Williams,[1] L. DiCarlo,[2] C. M. Marcus[2]*

The unique band structure of graphene allows reconfigurable electric-field control of carrier type and density, making graphene an ideal candidate for bipolar nanoelectronics. We report the realization of a single-layer graphene *p-n* junction in which carrier type and density in two adjacent regions are locally controlled by electrostatic gating. Transport measurements in the quantum Hall regime reveal new plateaus of two-terminal conductance across the junction at 1 and $\frac{3}{2}$ times the quantum of conductance, e^2/h, consistent with recent theory. Beyond enabling investigations in condensed-matter physics, the demonstrated local-gating technique sets the foundation for a future graphene-based bipolar technology.

Graphene, a single-layer hexagonal lattice of carbon atoms, has recently emerged as a fascinating system for fundamental studies in condensed-matter physics (*1*), as well as a candidate for novel sensors (*2*, *3*) and postsilicon electronics (*4–10*). The unusual band structure of single-layer graphene makes it a zero-gap semiconductor with a linear (photon-like) energy-momentum relation near the points where valence and conduction bands meet. Carrier type—electron-like or holelike—and density can be controlled by using the electric-field effect (*10*), obviating conventional semiconductor doping, for instance via ion implantation. This feature, doping via local gates, would allow graphene-based bipolar technology devices comprising junctions between holelike and electron-like regions, or *p-n* junctions, to be reconfigurable using only gate voltages to distinguish *p* (hole-like) and *n* (electron-like) regions within a single sheet. Although global control of carrier type and density in graphene using a single back gate has been investigated by several groups (*11–13*), local control (*8*, *9*) of single-layer graphene has remained an important technological milestone. In addition, *p-n* junctions are of great interest for low-dimensional condensed-matter physics. For instance, recent theory predicts that a local step in potential would allow solid-state realizations of relativistic (Klein) tunneling (*14*, *15*) and a surprising scattering effect known as Veselago lensing (*16*), comparable to scattering of electromagnetic waves in negative-index materials (*17*).

We report the realization of local top gating in a single-layer graphene device that, combined with global back gating, allows individual control of carrier type and density in adjacent regions of a single atomic layer. Transport measurements at zero perpendicular magnetic field *B* and in the quantum Hall (QH) regime demonstrate that the functionalized aluminum oxide (Al_2O_3) separating the graphene from the top gate does not significantly dope the layer nor affect its low-frequency transport properties. We studied the QH signature of the graphene *p-n* junction and found new conductance plateaus at 1 and $\frac{3}{2} e^2/h$, consistent with recent theory addressing equilibration of edge states at the *p-n* interface (*18*).

Graphene sheets were prepared via mechanical exfoliation using a method (*19*) similar to that used in (*10*). Graphite flakes were deposited on 300 nm of SiO_2 on a degenerately doped Si substrate. Inspection with an optical microscope allowed potential single-layer regions of graphene to be identified by a characteristic coloration that arises from thin-film interference (Fig. 1A). These micrometer-scale regions were contacted with thermally evaporated Ti/Au (5/40 nm) that was patterned using electron-beam lithography. Next, a ~30-nm layer of oxide was deposited atop the entire substrate. As illustrated (Fig. 1B), the oxide consisted of two parts, a nonconvalent functionalization layer (NCFL) and Al_2O_3. This deposition technique (*19*) was based on a recipe successfully applied to carbon nanotubes (*20*). The NCFL serves two purposes. One is to create a noninteracting layer between the graphene and the Al_2O_3, and the other is to obtain a layer that is catalytically suitable for the formation of Al_2O_3 by atomic layer deposition (ALD). The NCFL was synthesized by 50 pulsed cycles of NO_2 and trimethylaluminum (TMA) at room temperature inside an ALD reactor. Next, five cycles of H_2O-TMA were applied at room temperature to prevent desorption of the NCFL. Lastly, Al_2O_3 was grown at 225°C with 300 H_2O-TMA ALD cycles. To complete the device, a second step of electron-beam lithography defined a local top gate (5/40 nm Ti/Au) covering a region of the device that includes one of the metallic contacts.

A completed device, similar in design to that shown in the optical image in Fig. 1A, was cooled in a ^{3}He3 refrigerator and characterized at temperatures *T* of 250 mK and 4.2 K. Differential resistance, $R = dV/dI$, where *I* is the current and *V* the source-drain voltage, was measured by standard lock-in techniques with a current bias

[1]School of Engineering and Applied Science, Harvard University, Cambridge, MA 02138, USA. [2]Department of Physics, Harvard University, Cambridge, MA 02138, USA.

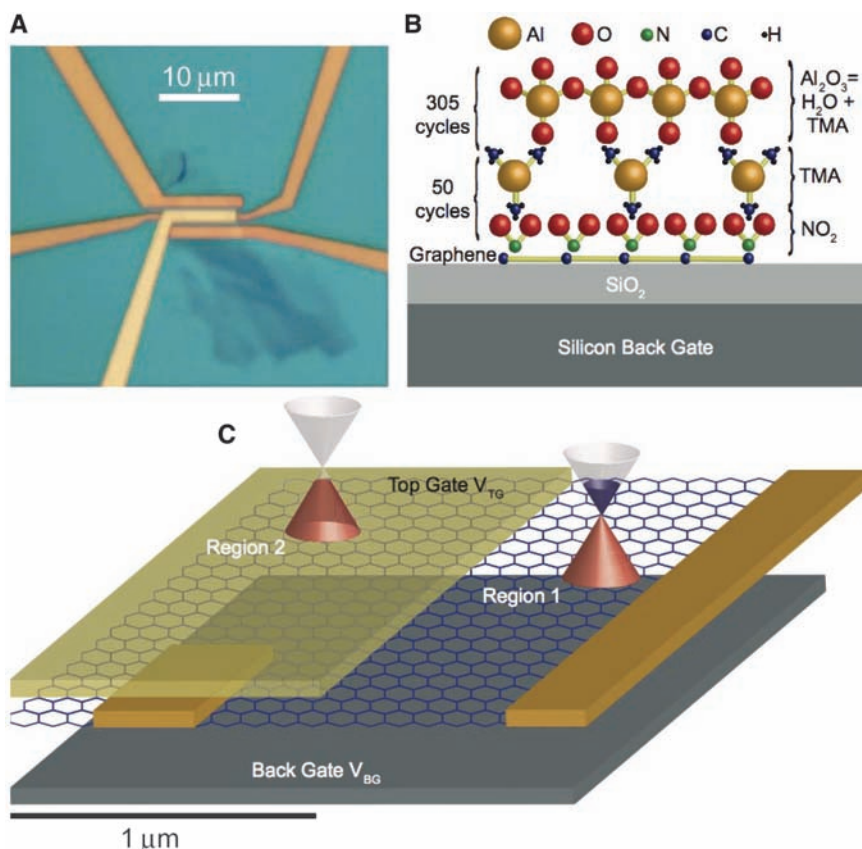*To whom correspondence should be addressed. E-mail: marcus@harvard.edu

Fig. 1. (**A**) Optical micrograph of a device similar to the one measured. Metallic contacts and top gate appear in orange and yellow, respectively. Darker regions below the contacts are thicker graphite from which the contacted single layer of graphene extends. (**B**) Illustration of the oxide deposition process. A noncovalent functionalization layer is first deposited with NO_2 and TMA (50 cycles), and Al_2O_3 is then grown by ALD using H_2O-TMA (305 cycles yielding ~30-nm thickness). (**C**) Schematic of the device measured in this experiment.
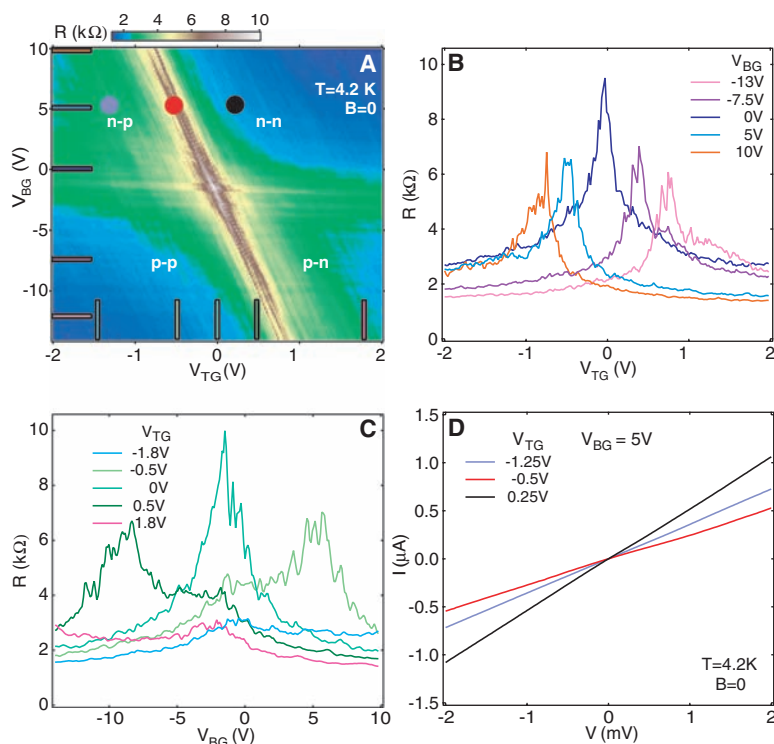
of 1 nA_{rms} at 95 Hz for $T = 250$ mK and 10 nA_{rms} for $T = 4.2$ K. The voltage across two contacts on the device, one outside the top-gate region and one underneath the top gate, was measured in a four-wire configuration, eliminating series resistance of the cryostat lines but not contact resistance. Contact resistance was evidently low (~1 kohm), and no background was subtracted from the data. A schematic of the device is shown in Fig. 1C.

The differential resistance, R, as a function of back-gate voltage, V_{BG}, and top-gate voltage, V_{TG}, at $B = 0$ (Fig. 2A) demonstrates independent control of carrier type and density in the two regions. This two-dimensional (2D) plot reveals a skewed, crosslike pattern that separates the space of top-gate and back-gate voltages into four quadrants of well-defined carrier type in the two regions of the sample. The horizontal and diagonal ridges correspond to charge neutrality, i.e., the Dirac point, in regions 1 and 2, respectively. The slope of the charge-neutral line in region 2, along with the known distances to the top gate and back gate gives a dielectric constant $\kappa \sim 6$ for the functionalized Al_2O_3. The center of the cross at (V_{TG}, V_{BG}) ~ (−0.2 V, −2.5 V) corresponds to charge neutrality across the entire graphene sample. Its proximity to the origin of gate voltages demonstrates that the functionalized oxide does not chemically dope the graphene substantially.

Slices through the 2D conductance plot at fixed V_{TG} are shown in Fig. 2C. The slice at $V_{TG} = 0$ shows a single peak commonly observed in devices with only a global back gate (10–13). By using a Drude model away from the charge-neutrality region, we estimated mobility at ~7000 cm^2/Vs (10). The peak width, height, and back-gate position are consistent with single-layer graphene (11–13) and

Fig. 2. (**A**) Two-terminal differential resistance R as a function of V_{TG} and V_{BG} at $B = 0$ and $T = 4.2$ K, demonstrating independent control of carrier type and density in regions 1 and 2. Labels in each of the four quadrants indicate the carrier type (first letter indicates carrier type in region 1). (**B** and **C**) Horizontal slices at V_{BG} and vertical slices at V_{TG}; settings corresponding to the colored lines superimposed on Fig. 2A. (**D**) I-V curves at the gate voltage settings corresponding to the solid circles in Fig. 2A are representative of the linear characteristics observed everywhere in the plane of gate voltages.

provide evidence that the electronic structure and degree of disorder of the graphene are not strongly affected by the oxide. Slices at finite $|V_{TG}|$ reveal a doubly peaked structure. The weaker peak, which remains near $V_{BG} \sim -2.5$ V at all V_{TG}, corresponds to the Dirac point of region 1. The stronger peak, which moves linearly with V_{TG}, is the Dirac point for region 2. The difference in peak heights is a consequence of the different aspect ratios of regions 1 and 2. Horizontal slices at fixed V_{BG} corresponding to the horizontal lines in Fig. 2A are shown in Fig. 2B. These slices show a single peak, corresponding to the Dirac point of region 2. This peak becomes asymmetric away from the charge-neutrality point in region 1. We note that the V_{BG} dependence of the asymmetry is opposite to that observed in (9), where the asymmetry is studied in greater detail. The changing background resistance results from the different density in region 1 at each V_{BG} setting. Current-voltage (I-V) characteristics, measured throughout the (V_{TG}, V_{BG}) plane, show no sign of rectification in any of the four quadrants or at either of the charge-neutral boundaries between quadrants (Fig. 2D), as expected for reflectionless (Klein) tunneling at the p-n interface (14, 15).

In the QH regime at large B, the Dirac-like energy spectrum of graphene gives rise to a char-

acteristic series of QH plateaus in conductance, reflecting the presence of a zero-energy Landau level that includes only odd multiples of $2e^2/h$ (that is, 2, 6, 10,... × e^2/h) for uniform carrier density in the sheet (21–23). These plateaus can be understood in terms of an odd number of QH edge states (including a zero-energy edge state) at the edge of the sheet, circulating in a direction determined by the direction of B and the carrier type. The situation is somewhat more complicated when varying local density and carrier type across the sample.

A 2D color plot of differential conductance $g = 1/R$ as a function of V_{BG} and V_{TG} at $B = 4$ T is shown in Fig. 3A. A vertical slice at $V_{TG} = 0$ through the p-p and n-n quadrants (Fig. 3B) reveals conductance plateaus at 2, 6, and $10e^2/h$ in both quadrants, demonstrating that the sample is single layer and that the oxide does not significantly distort the Dirac spectrum.

QH features are investigated for differing filling factors ν_1 and ν_2 in regions 1 and 2 of the graphene sheet. A horizontal slice through Fig. 3A at filling factor $\nu_1 = 6$ is shown in Fig. 3C. Starting from the n-n quadrant, plateaus are observed at $6e^2/h$ and $2e^2/h$ at top-gate voltages, corresponding to filling factors $\nu_2 = 6$ and $\nu_2 = 2$, respectively. Crossing over to the n-p quadrant by further decreasing V_{TG}, a new plateau at $\frac{3}{2}e^2/h$

appears for $\nu_2 = -2$. In the $\nu_2 = -6$ region, no clear QH plateau is observed. Another horizontal slice at $\nu_1 = 2$ shows $2e^2/h$ plateaus at both $\nu_2 = 6$ and $\nu_2 = 2$ (Fig. 3D). Crossing into the n-p quadrant, the conductance exhibits QH plateaus at $1e^2/h$ for $\nu_2 = -2$ and near $\frac{3}{2}e^2/h$ for $\nu_2 = -6$.

For ν_1 and ν_2 of the same sign (n-n or p-p), the observed conductance plateaus follow

$$g = min(|\nu_1|, |\nu_2|) \times 2e^2/h \qquad (1)$$

This relation suggests that the edge states common to both regions propagate from source to drain, whereas the remaining $|\nu_1 - \nu_2|$ edge states in the region of highest absolute filling factor circulate internally within that region and do not contribute to the conductance. This picture is consistent with known results on conventional 2D electron gas systems with inhomogeneous electron density (24–26).

Recent theory (18) addresses QH transport for filling factors with opposite sign in regions 1 and 2 (n-p and p-n). In this case, countercirculating edge states in the two regions travel in the same direction along the p-n interface (Fig. 3F), which presumably facilitates mode mixing between parallel-traveling edge states. For the case of complete mode mixing, that is, when current entering the junction region becomes uniformly distributed among the $|\nu_1| + |\nu_2|$ parallel-traveling modes, quantized plateaus are expected (18) at values

$$g = \frac{|\nu_1||\nu_2|}{|\nu_1| + |\nu_2|} \times 2e^2/h \qquad (2)$$

A table of the conductance plateau values given by Eqs. 1 and 2 is shown in Fig. 3E. Plateau values at $1e^2/h$ for $\nu_1 = -\nu_2 = 2$ and at $\frac{3}{2}e^2/h$ for $\nu_1 = 6$ and $\nu_2 = -2$ are observed in the experiment. Notably, the $\frac{3}{2}e^2/h$ plateau suggests uniform mixing among four edge stages (three from region 1 and one from region 2). All observed conductance plateaus are also seen at $T = 4$ K and for B in the range from 4 to 8 T [Supporting Online Material (SOM) text].

We do find some departures between the experimental data and Eqs. 1 and 2, as represented in the grid of Fig. 3E. For instance, the plateau near $\frac{3}{2}e^2/h$ in Fig. 3D is seen at a value of $\sim 1.4e^2/h$, and no clear plateau at $3e^2/h$ is observed for $\nu_1 = -\nu_2 = 6$. We speculate that the conductance in these regions being lower than their expected values is an indication of incomplete mode mixing. We also observe an unexpected peak in conductance at a region in gate voltage between the two $1e^2/h$ plateaus at $\nu_1 = \pm\nu_2 = 2$. This rise in conductance is clearly seen for $|V_{TG}|$ values between ~ 1 and 2 V and V_{BG} values between ~ -5 and -2 V. This may result from the possible existence of puddles of electrons and holes near the charge-neutrality points of regions 1 and 2, as previously suggested (27).
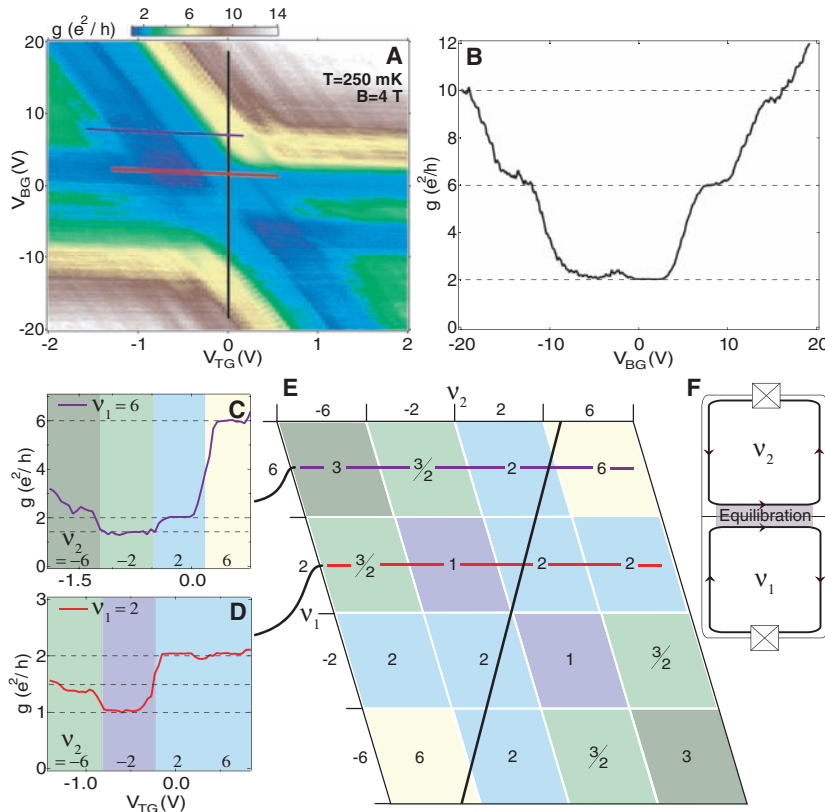

Fig. 3. (**A**) Differential conductance g as a function of V_{TG} and V_{BG} at $B = 4$ T and $T = 250$ mK. (**B**) Vertical slice at $V_{TG} = 0$, traversing p-p and n-n quadrants. Plateaus are observed at $2e^2/h$ and $6e^2/h$, the QH signature of single-layer graphene. (**C**) Horizontal slice at $\nu_1 = 6$ showing conductance plateaus at 6, 2, and $\frac{3}{2}e^2/h$. (**D**) Horizontal slice at ν_2 showing QH plateaus at 2, 1, and $\frac{3}{2}e^2/h$. (**E**) Table of conductance plateau values as a function of filling factors calculated with Eqs. 1 and 2. Black, purple, and red lines correspond to slices in (B), (C), and (D), respectively. (**F**) Schematic of countercirculating edge states at filling factors $\nu_1 = -\nu_2 = 2$.

References and Notes
1. A. K. Geim, K. S. Novoselov, *Nat. Mater.* **6**, 183 (2007).
2. F. Schedin *et al.*, http://arxiv.org/abs/cond-mat/0610809.

3. E. H. Hwang, S. Adam, S. Das Sarma, A. K. Geim, http://arXiv.org/abs/cond-mat/0610834.
4. C. Berger *et al.*, *Science* **312**, 1191 (2006); published online 12 April 2006 (10.1126/science.1125925).
5. Z. Chen, Y.-M. Lin, M. J. Rooks, P. Avouris, http://arXiv.org/abs/cond-mat/0701599.
6. M. Y. Han, B. Özyilmaz, Y. Zhang, P. Kim, http://arXiv.org/abs/cond-mat/0702511.
7. A. Rycerz, J. Tworzydło, C. W. J. Beenakker, *Nature Phys.* **3**, 172 (2007).
8. M. C. Lemme, T. J. Echtermeyer, M. Baus, H. Kurz, *IEEE Electron Device Lett.* **28**, 283 (2007).
9. B. Huard *et al.*, *Phys. Rev. Lett.* **98**, 236803 (2007).
10. K. S. Novoselov *et al.*, *Science* **306**, 666 (2004).
11. K. S. Novoselov *et al.*, *Nature* **438**, 197 (2005).
12. Y. Zhang, Y.-W. Tan, H. Stormer, P. Kim, *Nature* **438**, 201 (2005).
13. H. B. Heersche, P. Jarillo-Herrero, J. B. Oostinga, L. M. K. Vandersypen, A. F. Morpurgo, *Nature* **446**, 56 (2007).
14. M. I. Katsnelson, K. S. Novoselov, A. K. Geim, *Nature Phys.* **2**, 620 (2006).
15. V. V. Cheianov, V. I. Fal'ko, *Phys. Rev. B* **74**, 041403(R) (2006).
16. V. V. Cheianov, V. Fal'ko, B. L. Altshuler, *Science* **315**, 1252 (2007).
17. D. R. Smith, J. B. Pendry, M. C. K. Wiltshire, *Science* **305**, 788 (2004).
18. D. A. Abanin, L. S. Levitov, *Science* **317**, 641 (2007).
19. Information on materials and methods is available on *Science* Online.
20. D. B. Farmer, R. G. Gordon, *Nano Lett.* **6**, 699 (2006).
21. P. Gusynin, S. G. Sharapov, *Phys. Rev. Lett.* **95**, 146801 (2005).
22. A. Abanin, P. A. Lee, L. S. Levitov, *Phys. Rev. Lett.* **96**, 176803 (2006).
23. N. M. R. Peres, F. Guinea, A. H. Castro Neto, *Phys. Rev. B* **73**, 125411 (2006).
24. D. A. Syphers, P. J. Stiles, *Phys. Rev. B* **32**, 6620 (1985).
25. R. J. Haug, A. H. MacDonald, P. Streda, K. von Klitzing, *Phys. Rev. Lett.* **61**, 2797 (1988).
26. S. Washburn, A. B. Fowler, H. Schmid, D. Kern, *Phys. Rev. Lett.* **61**, 2801 (1988).
27. E. H. Hwang, S. Adam, S. Das Sarma, *Phys. Rev. Lett.* **98**, 186806 (2007); also available at http://arXiv.org/abs/cond-mat/0610157.
28. We thank L. S. Levitov, D. A. Abanin, C. H. Lewenkopf, and P. Jarillo-Herrero for useful discussions; Z. Chen at IBM T. J. Watson Research Center for suggesting the NO$_2$ functionalization process; and D. Monsma for assistance in implementing it. Research supported in part by INDEX and by the NSF through the Harvard Nanoscale Science and Engineering Center.

Quantized Transport in Graphene *p-n* Junctions in a Magnetic Field

D. A. Abanin and L. S. Levitov*

Recent experimental work on locally gated graphene layers resulting in *p-n* junctions has revealed the quantum Hall effect in their transport behavior. We explain the observed conductance quantization, which is fractional in the bipolar regime and an integer in the unipolar regime, in terms of quantum Hall edge modes propagating along and across the *p-n* interface. In the bipolar regime, the electron and hole modes can mix at the *p-n* boundary, leading to current partition and quantized shot-noise plateaus similar to those of conductance, whereas in the unipolar regime transport is noiseless. These quantum Hall phenomena reflect the massless Dirac character of charge carriers in graphene, with particle/hole interplay manifest in mode mixing and noise in the bipolar regime.

The transport properties of graphene [two-dimensional sheets of graphite (*1*)], in particular the high carrier mobility and tunability of transport characteristics, make this material attractive for applications in nanoelectronics (*2*, *3*). Various methods have been developed for patterning graphene sheets into prototype devices such as quantum-dot transistors (*1*) and nanoribbons (*4*, *5*), followed by the demonstration of local control of carrier density in a graphene sheet (*6*). Besides possible device applications, graphene junctions are predicted to host new and exciting phenomena reflecting the massless Dirac character of carriers in this material, such as Klein tunneling (*7*), particle collimation (*8*), quasibound states (*9*), and Veselago lensing (*10*). In addition, interesting phenomena are expected in gated graphene bilayers, where field-effect transport can be induced by tuning the gap at the Dirac point (*11*). These applications make the gating of graphene a topic of great interest.

Recently, a graphene *p-n* junction with individual control of carrier density in two adjacent regions with a pair of gates above and below it was reported (*12*). The density in each region could be varied across the neutrality point, allowing *p-n*, *p-p*, and *n-n* junctions to be formed at the interface. The interface width was quite small, owing to the 30-nm distance to the top gate and its sharp edge. Transport measurements, carried out in the quantized Hall effect (QHE) regime at magnetic fields $3\,\mathrm{T} < B < 8\,\mathrm{T}$, revealed ohmic two-terminal conductance taking quantized values $g = 6, 2, \frac{3}{2}$, and 1 in the units of conductance quantum e^2/h, where h is Planck's constant. The QHE plateaus with $g = 2$ and 6 were observed in the unipolar regime, whereas the quantized plateaus with $g = 1$ and $\frac{3}{2}$ of similar quality were observed in the bipolar regime. Whereas conductance of $6e^2/h$ and $2e^2/h$ is a hallmark of the integer QHE in graphene (*13*, *14*), quantized conductance values of $\frac{3}{2}$ and 1 are unusual and call for explanation.

We interpret these observations by linking them to the properties of the Dirac-like carriers, which give rise to bipolar electron and hole QHE edge modes at the *p-n* interface (Fig. 1). The behavior at the interface is explained by employing ideas from the theory of quantum-chaotic transport (*15–20*). Although in our case the edge modes carry charge along the *p-n* interface all in the same direction (in a chiral rather than chaotic fashion), we argue that intermode scattering within the *p-n* interface region gives rise to dynamics with features analogous to those known for quantum-chaotic systems.

In this analogy, the QHE states at the sample boundary play the role of perfect lead channels of chaotic quantum dots (*15*, *16*), bringing charge to the *p-n* interface and carrying it away into reservoirs. However, several physical effects causing conductance fluctuations in chaotic dots are absent in our case, leading to quantization of two-terminal conductance not known for the dots. In particular, the effective lead channels are quantized more perfectly than in the dots, owing to backscattering suppression in QHE transport. In addition, the quantum-mechanical interference effects, which lead to sample-specific conductance fluctuations, can be suppressed in our case because of self-averaging, as well as dephasing and electron-electron scattering. Other effects that can affect the edge-state transport at the *p-n* interface are

Fig. 1. Schematic of QHE edge states for the (**A**) bipolar regime and (**B**) unipolar regime of a graphene junction. In (A), the edge states counter-circulate in the *n* and *p* regions, bringing elec-

trons and holes from different reservoirs to the *p-n* interface. Mode mixing at the interface leads to the two-terminal conductance (Eq. 1). In (B), because the edge states circulate in the same direction without backscattering or mixing, conductance is determined by the modes permeating the whole system, $g = \min(|\nu_1|, |\nu_2|)$.
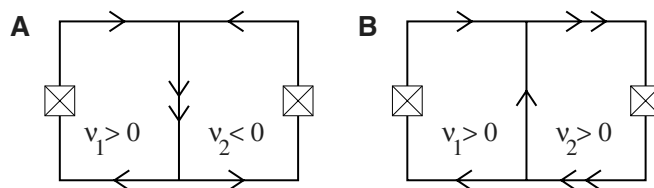
Department of Physics, Center for Materials Sciences and Engineering, Massachusetts Institute of Technology, 77 Massachusetts Avenue, Cambridge, MA 02139, USA.

*To whom correspondence should be addressed. E-mail: levitov@mit.edu

Science

AAAS